RESEARCH ARTICLE

ADVANCED OPTICAL MATERIALS
www.advopticalmat.de

Enhanced Circularly Polarized Lasing in Nanocellulose-Silica Composites

Sunghwan Jo, Irene Estévez, Angel Lizana, Juan Campos, and Agustin Mihi**

Crystalline nanocellulose (CNC) is a nanometric form of cellulose known for its cholesteric structure, imparting circular dichroism to the material. CNC has been used in many photonic applications, exploiting its chiroptical properties to produce circularly polarized photoluminescence. In this work, an insightful characterization of the polarimetric response of nanocrystalline cellulose created through the scalable process of vacuum filtration is performed. This study confirms the strong dichroic character of the nanocellulose films but also reveals a significant linear dichroism contribution, which in turn limits the use of the material to produce a higher degree of circularly polarized light. Here, it is demonstrated that the incorporation of silica nanospheres into the CNC matrix significantly reduces the linear dichroism in the film. More importantly, the decrease in linear diattenuation correlates with an increase in circular dichroism, leading to samples with improved performance as circular polarizers (circular diattenuator). The enhanced chiroptical response of the silica-nanocellulose composites is demonstrated by building a chiral lasing system consisting of a thin layer of resist containing an organic dye (rhodamine B) enclosed between two layers of nanocrystalline cellulose. A maximum photoluminescence dissymmetry factor of 0.57 is observed at the wavelength of 611 nm.

1. Introduction

Circularly polarized (CP) light has received significant attention over the past few decades for its use in fields such as advanced optical communication,[1] data storage,[2] 3D displays,[3] and even medical imaging and therapeutic techniques,[4] where the properties of polarization can have a crucial impact. CP light can be generated by placing different optical components after an unpolarized light source, however, this strategy necessarily introduces brightness losses and limits device miniaturization. New methods for generating circular polarization, free from these restrictions, include the use of different photonic nanostructures combined with active media,[5–9] or directly producing chiral luminophores via chemical approaches.[10–12] Circularly polarized lasing systems have also been developed, for instance, by combining organic dyes with chiral plasmonic colloids[13] however, the highest fractions of CP light have typically been achieved by embedding the gain media within the chiral nematic structure of a cholesteric liquid crystal (CLC).[3] This latter approach achieved up to a 50% polarization asymmetry, as indicated by photoluminescence dissymmetry factors (g_{lum}) exceeding 1($g_{lum} = (I_{LCP}-I_{RCP})/0.5^{*}(I_{LCP}+I_{RCP})$). However, working with CLC requires additional insulating layers to prevent leakage of the CLC and to ensure the structural integrity of the device.

Among the materials showing a CLC phase, crystalline nanocellulose (CNC) stands out for being a cellulose derivative, the most abundant biopolymer in nature.[14] CNC is a needle-like nanoparticle (NP) that can be obtained through mechanical, chemical, or enzymatic treatments performed on raw cellulose.[14,15] Dried CNC has no absorption in the visible spectral range,[16] still CNC films display structural color and circular dichroism (CD) originated by the self-assembled cholesteric structure which consists of a left-handed helix with several hundred nanometers pitch. CNC films have quickly been sought for its nature-originated aspect and CD properties. The optical properties of CNC films can be tuned by altering the helical pitch length or the alignment of the nanocrystals by adding polymers,[17,18] sonication energy,[19,20] external electric or magnetic fields,[21,22] and pH.[23] The chiral-responsive structural color can be exploited for biodegradable pigments,[24] colorimetric sensors,[25] chiroptical waveguides for telecommunication fiber technology,[26] and information encryption.[15] Furthermore, CNC can be mixed with metal nanoparticles[27] or a host of fluorophores to produce right-handed CP light[28–32] very efficiently. Lasing in CNC films has been also shown to exhibit a notable degree of circular dichroism,[30] however, the fraction of polarized PL observed is still below those measured in CLCs, indicating the need for a novel approach to enhance it. In general, the polarizing capability of a medium is assessed in terms of Kuhn's

S. Jo, A. Mihi
Institute of Materials Science of Barcelona ICMAB-CSIC
Campus UAB Bellaterra, Bellaterra 08193, Spain
E-mail: sunghwanjo@icmab.es; amihi@icmab.es
I. Estévez, A. Lizana, J. Campos
Grupo de Óptica
Departamento de Física
Universitat Autònoma de Barcelona UAB
Bellaterra 08193, Spain

The ORCID identification number(s) for the author(s) of this article can be found under https://doi.org/10.1002/adom.202500212

DOI: 10.1002/adom.202500212

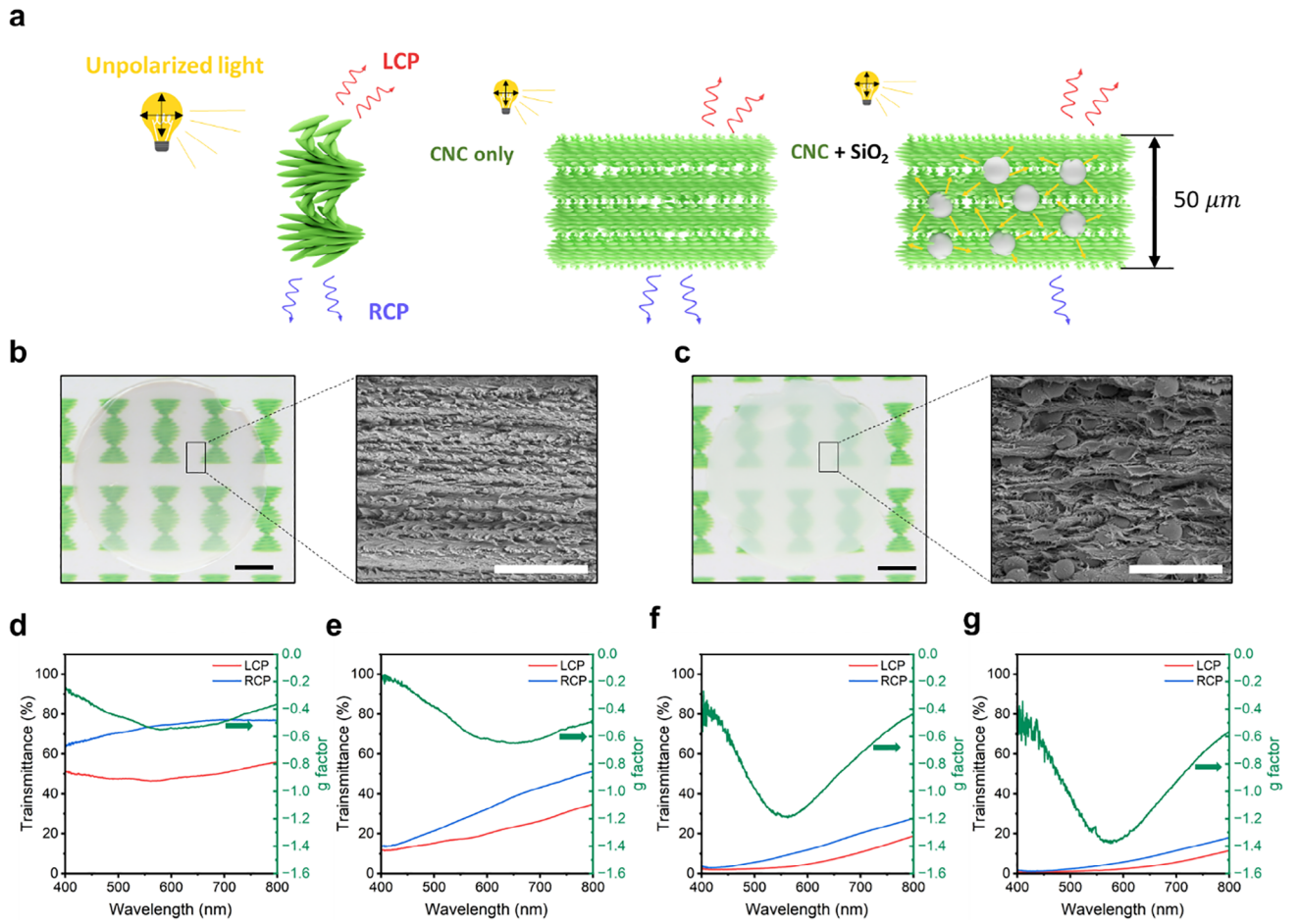

Figure 1. a) Schematics of self-assembled CNC: a bare CNC film versus a SiO_2-CNC composite. The left-handed cholesteric structure of the CNC shows a circular dichroic response, which can be combined with the high scattering of 600 nm SiO_2 NPs. Photographs and SEM images from b) CNC film, and c) SiO_2-CNC composite (with $[SiO_2] = 4$ wt.%) films. d) Transmittance spectra under LCP and RCP light and their corresponding dissymmetry factors (g-factors) for a bare CNC film and e) SiO_2-CNC composite films with different $[SiO_2] = 1.25$ wt.%, f) 2.5 wt.%, and g) 4 wt.% respectively.

dissymmetry factor or g-factor, which quantifies asymmetries in the extinction of light passing through the material.

However, a more complete characterization of the optical response, albeit less commonly used, of the material can be achieved by using the Mueller matrix (MM) description. In the context of CNC, only a few studies in the literature have examined this material using the MM framework.[27,33,34]

In this work, we use Mueller matrix characterization to understand the optical response of CNC films made by the scalable approach of vacuum filtration. The polarimetric study revealed that in addition to the strong circular dichroism response from the CNC films, a relevant linear dichroism component is also present, thus limiting the purely chiroptical response of the material. Here, we exploit the resilient character of circular polarization over other polarization states. To achieve this, we incorporate silica nanospheres into the CNC matrix as scatterers, selectively reducing the linear dichroic contribution. Our silica-CNC composites show an improved g-factor and negligible linear dichroism in polarimetric studies than bare CNC films. Next, these silica-CNC films are utilized to provide optical feedback from a rhodamine B (RhB)-doped photoresist thin film, enabling the generation of chiral lasing emission. We assessed the light amplification effect induced by the 600 nm SiO_2 NPs by measuring the pumping energy-dependent photoluminescence (PL) for different sphere concentrations. Also, we characterize the angular dispersion and directionality of the lasing emission. The PL from the dye showed a substantial degree of g_{lum} up to 0.6. Moreover, the SiO_2-CNC lasing systems provide a preferential left-handed CP light feedback, which results in a positive g_{lum}, coinciding with the reflection band associated with the CNC-based light amplification effect.

2. Results and Discussion

CNC films featuring a left-handed cholesteric structure were fabricated via a vacuum filtration method, a method much faster than the evaporation-assisted self-assembly process (4 h vs 3 days), rendering CNC films that can be easily handled and transferred onto other surfaces.[20] We selected vacuum filtration over self-assembly for producing CNC films due to its superior scalability, less production time (from several days to a few hours), and suitability for consistent and large-scale manufacturing.[20]

We produced a series of CNC films (50 µm thickness) containing different concentrations of 600 nm-diametered SiO_2 spheres (from 0 to 4 wt.%) (**Figure 1a**) previously produced by the Stöber method (See Experimental section).[35] The role of the silica beads in the CNC matrix is to reduce the linear dichroism contribution, thus increasing the degree of CP obtained.[36,37]

Bare CNC films exhibit high transparency (Figure 1b), which gradually diminishes with the incorporation of SiO_2 nanospheres into the CNC matrix (Figure 1c). It is worth noting that for the silica concentrations considered in this study, the incorporation of the 600 nm SiO_2 spheres in the CNC matrix does not induce any phase separation or disrupt the cholesteric structure (Figure 1c). The first transmittance measurements were performed using a custom optical setup, measuring the transmittance for both left and right-handed circular polarized light (LCP and RCP, respectively) through the composite films (Figure S6, Supporting Information). From these measurements, we calculated the dissymmetry factor (g-factor) using the formula: $g = (T_L - T_R)/0.5^{*}(T_L + T_R)$, where T_L and T_R are the transmittance by LCP and RCP input light.[5] Increasing the silica content in the 50 µm-CNC film reduces the overall transmittance, especially for the LCP light, which at 600 nm significantly decreases from 47.2% to 2.3% (for the RCP light a reduction from 74.7% to 5.7% is found), which results in a negative g-factor (Figure 1d–g) that increases with the concentration of SiO_2 NP (g-factor = −0.54 for 0 wt.%, and −0.64 for 1.25 wt.%, −1.10 2.5 wt.%, and −1.34 for 4 wt.% at 600 nm). Further increasing the SiO_2 NP concentration over 4 wt.% makes the film brittle, causing it to break and preventing further assessment of potential saturation effects.

The transmittance results show how the g-factor increases by adding the SiO_2 scatterers. For a better interpretation of this result, the previous study is complemented with a polarimetric analysis.

Within the Mueller–Stokes formalism framework, the Mueller matrix, a 4 × 4 matrix with real elements, is a powerful tool for analyzing the main polarimetric features of samples, such as dichroism, birefringence, or depolarization. This 4 × 4 matrix provides a comprehensive description of polarimetric light-matter interactions, including changes in the polarization state produced by the medium. The Mueller matrix encodes all the physical characteristics related to the polarization of a sample. These can be analyzed through a set of polarimetric observables with clear physical interpretation, which can be directly deduced by operating on the Mueller matrix elements, as can be the case of the depolarization index (P_Δ) to analyze global depolarization induced by the media or the Diattenuation vector ($\vec{D}$), representing the dichroism features of the sample, among others. A full description of MM, including theoretical background, can be found in the experimental section Supporting Information. In this work, we implemented MM analysis to further investigate the left-handed and right-handed circular polarization transmission asymmetry seen in the CNC/SiO_2 composite films through the above-stated g-factor measurement, as well as some inherent polarimetric features contributing to this dependence. The experimental MM images were acquired by a custom-built optical setup (Complete Mueller matrix imaging polarimeter) consisting of a polarization state generator, a polarization state analyzer, and a 633 nm LED source with a bandpass filter in the transmission mode (Figure S3, Supporting Information). As stated above, in order to relate experimental MMs to the physical properties of the samples, appropriate data processing is essential. In this work, we retrieved three main characteristics of the samples, g-factor (closely connected to circular diattenuation), linear diattenuation (D_L), and P_Δ (to estimate global depolarization capability), from the MM images. The original MM images can be found in Figure S3 (Supporting Information). The depolarization index P_Δ is a well-known metric in depolarizing analysis and can be understood as a generalization of the degree of polarization in light beams applied to the depolarizing capability of the samples inspected. P_Δ ranges from 0 to 1, taking values of 1 for non-depolarizing systems and 0 for a completely depolarizing system, and can be defined as shown below,[38]

$$P_\Delta = \sqrt{\frac{\left(\sum_{i,j=0}^{3} m_{ij}^2\right) - m_{00}^2}{3m_{00}^2}} \tag{1}$$

where m_{00} is the so-called mean intensity coefficient, which represents the ratio between the intensity of the emerging light and the intensity of an incident unpolarized light, and m_{ij} are the matrix elements of the MM (i = 0, 1, 2, 3). Diattenuation represents different transmittance responses of material for different incident polarization states, enabling quantification of the polarizer's efficiency or diattenuation magnitude. Then, linear diattenuation (D_L) characterizes the anisotropy of the sample in transmission for input linear polarizations, as defined by the following equation,

$$D_L = \frac{\sqrt{m_{01}^2 + m_{02}^2}}{m_{00}} \tag{2}$$

where m_{01}, m_{02} elements describe the linear extinction at 0°/90° and 45°/135°, respectively ($0 \le D_L \le 1$). The g-factor we defined above can be also extracted from the MM as shown below,

$$g = \frac{-2m_{03}}{m_{00}} \tag{3}$$

where m_{03} is the element starting for circular dichroism.

Figure 2a presents the overall data for the g-factor, P_Δ, and D_L of the CNC/SiO_2 composites as a function of SiO_2 NP concentration, compiled from Figure 2b–d. The g-factors derived from the MM exhibit a trend consistent with those from the differential transmittance data, supporting the enhanced circular dichroic properties observed with increasing SiO_2 NP concentration (Figure 2d). Notably, D_L decreases significantly from 0.42 ± 0.04 at 0 wt.% SiO_2 to 0.06 ± 0.04 at 4 wt.% SiO_2. This decrease in D_L highlights the polarization-dependent attenuation effect in the CNC/ SiO_2 composites, suggesting that the addition of SiO_2 NPs in the CNC reduces the linear dichroism of the composite, thereby favoring the enhancement of circular dichroism. Conversely, P_Δ remains consistent at ≈0.8, indicating no significant depolarization effect due to the SiO_2 NPs. From these findings, we infer that as the SiO_2 concentration increases, the asymmetry in transmitted linear polarized light becomes negligible, while the asymmetry in transmitted circular polarized light significantly increases, providing the enhanced pure circular dichroic feature of the samples. This situation implies that, in

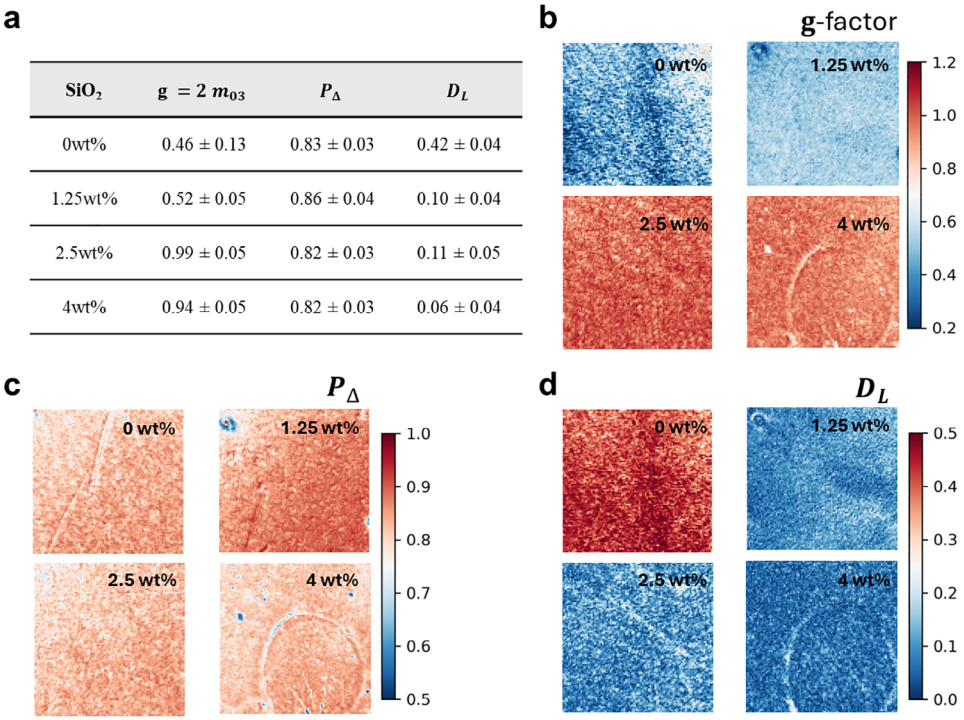

SiO_2	g $= 2\,m_{03}$	P_Δ	D_L
0wt%	0.46 ± 0.13	0.83 ± 0.03	0.42 ± 0.04
1.25wt%	0.52 ± 0.05	0.86 ± 0.04	0.10 ± 0.04
2.5wt%	0.99 ± 0.05	0.82 ± 0.03	0.11 ± 0.05
4wt%	0.94 ± 0.05	0.82 ± 0.03	0.06 ± 0.04

Figure 2. a) Summary of g-factor, depolarization index (P_Δ), and linear diattenuation (D_L) for CNC/SiO_2 composite films, all of which were obtained from Mueller matrix analysis. All data in this table is averaged from the polarimetric images for b) g-factor, c) P_Δ, and d) D_L.

the absence of other significant polarimetric phenomena, doping the CNC sample with SiO_2 nanospheres partially converts diattenuation from linear to circular.

In sum, increasing the SiO_2 concentration in the CNC matrix results in a decreased D_L of CP light transmission and a g-factor (reaching −1.33 for 4 wt.% SiO_2), which is an excellent candidate for creating a chiral lasing device with a high degree of circular polarization.

In previous studies, CNC has been used as host media for different emitters to achieve chiral light emission: Phosphor-doped latex nanoparticles, quantum dots, and rare-earth nanoparticles, for instance.[28,29,39–41] However, incorporating dyes into CNC composites can present certain disadvantages, such as phase separation due to additives, which disrupt the cholesteric structure, agglomeration leading to low luminescent intensity and uniformity,[28,39] and in the case of carbon quantum dots, a decrease in mechanical properties. To mitigate these issues, one solution is to encapsulate the fluorophores in a polymer matrix.[29,40] In this work, our gain medium is a thin film of Rhodamine B (RhB) doped resist, which is embedded within two CNC films (or in CNC/ RhB/ SiO_2 -CNC) as depicted in **Figure 3a**. This configuration of CNC/RhB/SiO_2-CNC enables exploiting the scattering properties of the silica-doped CNC within a chiral media to obtain chiral lasing seamlessly.

First, the light-emitting thin film was fabricated by spin-coating a 250 nm layer of RhB-doped photoresist (SU8 Microchem 2000.5) onto a 50 µm thick CNC film. Second, the CNC film with RhB is transferred onto partially wetted another CNC film (bare or SiO_2-CNC), and then it is left to dry to encapsulate the emitting layer (Figure 3a). Finally, the system is optically pumped through the bare CNC layer to avoid backscattering problems by SiO_2 NPs, and the PL is collected from the SiO_2-CNC side (Figure 3b). Full details on the fabrication of this lasing system can be found in the experimental section and Figure S1 (Supporting Information).

In Figure 3c–f we compare the g-factor and photoluminescence properties of the RhB doped resist layer embedded within CNC media versus the CNC/RhB/ 4% wt. SiO_2-CNC configuration. The absorption and emission characteristics of the dye, compared to the dichroism properties of each system, are presented in Figure 3c (CNC/RhB/CNC) and Figure 3e (CNC/RhB/4% wt. SiO_2-CNC). Figure 3d,f show the left-handed circularly polarized emission (LCP-E) spectra for both systems, CNC and CNC/SiO_2 (4 wt.%) composite film, respectively, as a function of energy density. In both cases, the PL intensity increases significantly when increasing optical fluences reaching a nonlinear character at 92.22 µJ mm^{-2} for 0 wt.% and 84 µJ mm^{-2} for 4 wt.% SiO_2 concentration in the CNC back layer. This trend shows how even in this configuration, in which the active layer and the scattering media are spatially separated, light amplification due to multiple scattering occurs. Moreover, the enhanced light amplification effect resulting from the polarization selective depolarization due to the added silica nanoparticles is evident from the change in the threshold point between 73.78 and 84.00 µJ mm^{-2} for 4 wt.% SiO_2. The PL intensity above the threshold for the silica-containing CNC is 5 times higher than the intensity for the bare CNC, even if it still shows a slightly lower threshold (3.2 for 0 wt.% and 3.69 for 4 wt.% SiO_2 -CNC, respectively).

The presence of SiO_2 spheres in the CNC matrix on the overall characteristics of the lasing emission was assessed in terms of

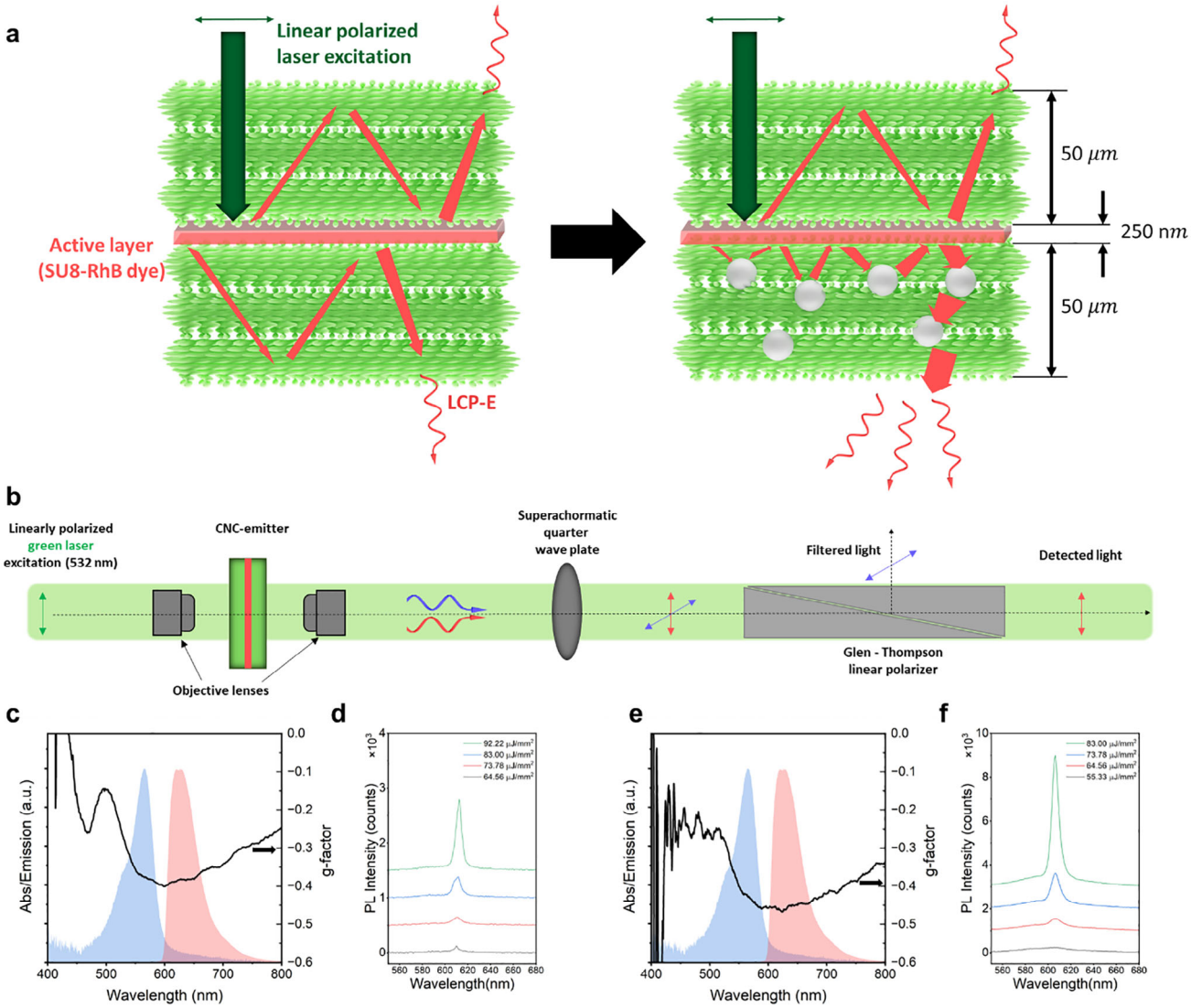

Figure 3. a) Schematic of the localized feedback configuration to obtain random lasing using CNC/RhB film/CNC and CNC/RhB film/CNC-SiO_2 films. b) Optical setup used to characterize the CD photoluminescence from the films. Normalized absorption (blue) and emission (red) spectra of a RhB-doped photoresist film on a glass substrate (left) and g-factors (right) of the c) CNC film and e) the SiO_2-doped (4 wt.%) CNC film. Photoluminescence spectra of the d) CNC/RhB/CNC and f) CNC/RhB/ CNC- SiO_2 (4 wt.%) composite films under different laser power densities.

the CPL intensity and the photoluminescence dissymmetry factor (g_{lum}) measured at different pumping energy densities. The g_{lum} is the magnitude used to evaluate the fraction of circularly polarized PL of a particular handedness produced by the system and is defined as $g_{lum} = (I_{LCP}\text{-}I_{RCP})/0.5^{*}(I_{LCP}+I_{RCP})$, where I_L and I_R represent the intensity of left and right circularly polarized PL emission.

According to the optical excitation fluence versus PL intensity plots, the spontaneous emission from the active material becomes stimulated emission regardless of the SiO_2 concentration in the second CNC layer. All configurations exhibit a threshold behavior for optical pumping ranging from 73.78 to 84 μJ mm^{-2}. Above this threshold, all systems exhibit a similar full width at half maximum (FWHM) of 5 to 8 nm (Figure S4, Supporting Information). However, the output intensity of LCP-E under the excitation of 110.67 μJ mm^{-2} for the CNC/RhB/ 4 wt.% SiO_2-CNC was 8.5 times higher than for the bare CNC system (Figure 3a). This result indicates that the presence of the SiO_2 spheres in the CNC matrix results in a higher lasing slope efficiency (21-fold for the 4% silica) with respect to the bare CNC case, meaning that the structure emits LCP light more efficiently above the threshold. The different slope efficiencies (LCP vs RCP) under different optical fluences can be found in the (Figure S5, Supporting Information). The increase in slope efficiency does not occur in the bare CNC system, even if higher film thicknesses (90 and 130 μm) are considered (Figure S7, Supporting Information).

Our chiral non linear emission with CNC films shows a positive g_{lum} (LCP dominant emission) unlike other CNC emitting configurations seen in the literature, which benefit RCP light (negative g_{lum}).[29,31,32,40] This is because the CNC films in our

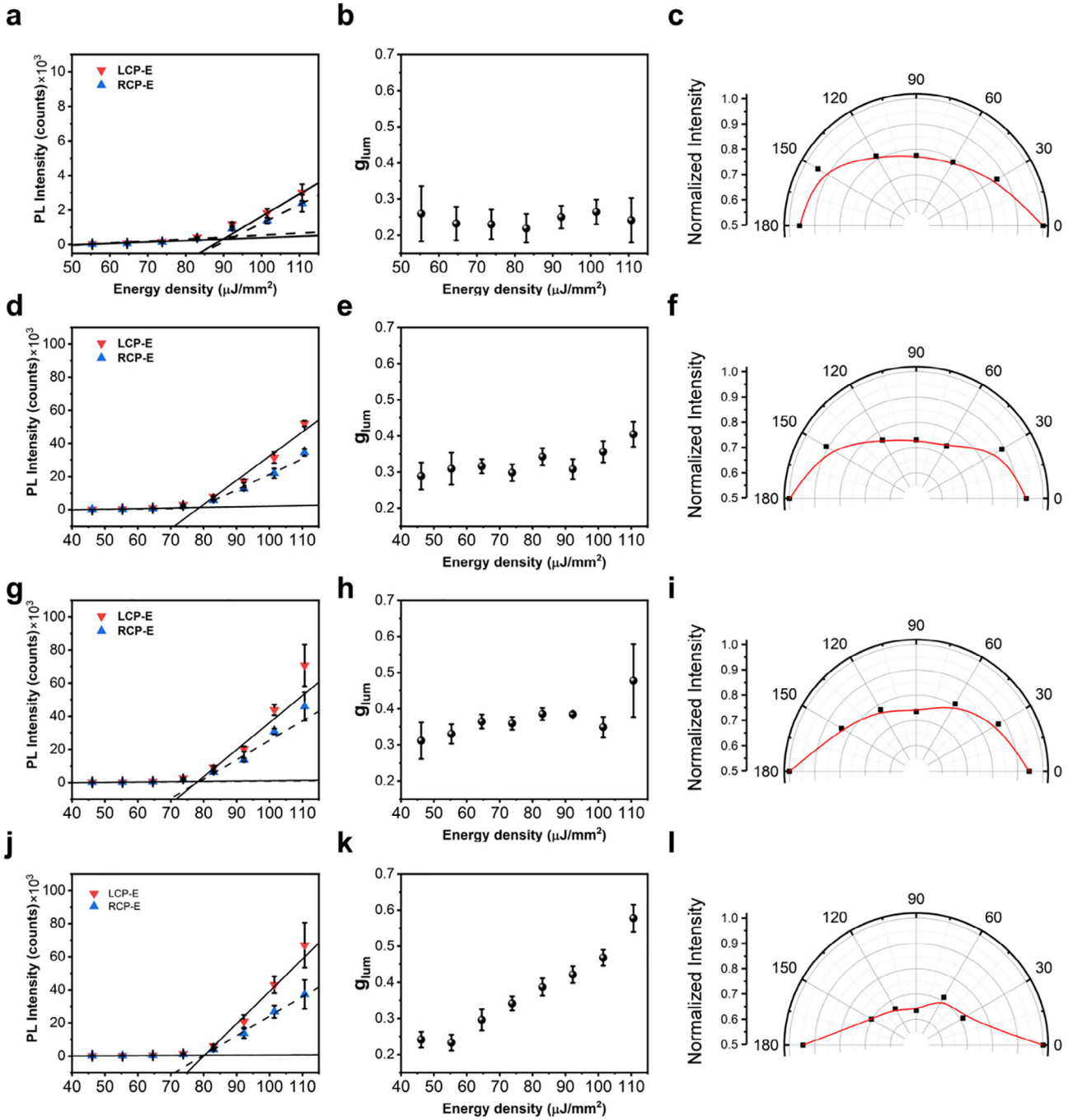

Figure 4. Photoluminescence intensity for Light (LCP-E) and Right (RCP-E) handed circularly polarized light and its corresponding g_{lum} (photoluminescence dissymmetry factor) for CNC/Rhodamine B/CNC films with different SiO_2 concentrations as a function of the pumping energy density. All CPL measurements were collected 5 times from each device. Polar plots of the left-handed circular polarization dependence were measured under 101.34 μJ mm^{-2} pump power and collected the emission through a quarter wave plate and a linear polarizer. (a–c, d–f, g–i, and j–l represent 0, 1.25, 2.5, and 4 wt.% of SiO_2, respectively).

configuration act as dielectric mirrors for left-handed light, effectively providing confinement and amplification for the LCP-E.[30]

The presence of silica spheres within the CNC layer also increased the magnitude of the g_{lum} at higher energy densities. Under an optical excitation of 110.67 μJ mm^{-2}, bare CNC films showed g_{lum} = 0.25 (**Figure 4b**), while it increased to 0.4 for the CNC- SiO_2 (1.25 wt.%) (Figure 4e) and CNC- SiO_2 (2.5 wt.%) (Figure 4i), reaching a maximum of g_{lum} = 0.57 for the CNC- SiO_2 (4 wt.%) system (Figure 4j). Furthermore, to evaluate the long-term stability of the system, CPL measurements were repeated on the same 4 wt.% device 4 months later. The CNC composite is sensitive to ambient humidity, which may distort the structure

under varying atmospheric conditions. However, provided that the active layer remains intact (i.e., no delamination occurs), the device retains ≈80% of its initial PL intensity, while the luminescence g_{lum} decreases by ≈50% (from 0.57 to 0.32), demonstrating acceptable stability (Figure S9, Supporting Information).

Next, we investigated the circular polarization characteristics of the photoluminescence produced in each system containing different SiO_2 concentrations (0, 1.25, 2.5, and 4 wt.%) on the backscattering CNC layer. The PL traveled through a quarter wave plate and a linear polarizer, and the intensity value was normalized to their maximum value at 101.34 μJ mm^{-2} and plotted with respect to the angle of the linear polarizer (schematics in Figure S10, Supporting Information). During the measurement, the f is converted into linearly polarized light in which 0° corresponds to an orientation of −45° with respect to the fast axis of the quarter-wave plate. These polar plots for circularly polarized light indicate that the emission transitions from less LCP light (fully unpolarized light corresponds to a semicircle in the plot) to a more circularly polarized state (Figure 4c,f,i,l) with increasing the silica content in the second CNC layer. This follows the same trend as the pumping energy density versus g_{lum} plot (Figure 4b,e,h,k), supporting the g_{lum} enhancement effect as the SiO_2 concentrations.

Conventional cavity lasers using metallic mirrors typically produce highly directional, non linear emissions. In contrast, our system employs a CNC/SiO_2 composite as a diffusive chiral mirror, which is expected to result in an emission pattern with distinct directional characteristics compared to traditional lasers. Therefore, we investigated the angular dispersion of the non linear emission from the CNC/RhB/CNC and CNC/RhB/CNC-SiO_2 films by rotating the photodetector from 0° to 85° with respect to the normal of the sample (full details in the setup in Figure S11, Supporting Information).

Figure 5a–d shows the evolution of the LCP-E with respect to the angle of observation and its corresponding g_{lum} values for the two main systems: CNC/RhB/CNC versus the best-performing silica-CNC system, the CNC/RhB/CNC-SiO_2(4 wt.%). Both configurations maintain a strong emission until an observation angle of 65° (Figure 5a,c). The values of the g_{lum} also decrease with the angle of observation from 0.2 to 0.1 for the bare CNC case and from 0.5 to 0.3 for the CNC/RhB/CNC- SiO_2 (4 wt.%) system (Figure 5b,d). This behavior can be attributed to the self-assembled structure of CNC, which resembles a chiral Bragg's stack with angle-dependent optical properties.[42] Interestingly, it is observed that the g_{lum} near the measurement angles of ±20 degrees is highest for both samples (Figure 5e,f). This suggests a trade-off point between the amplification due to light guiding in the in-plane direction of the device and the reduction in g_{lum} due to angle-dependent reflection as a result of increased scattering. Indeed, it can be noted that a significantly larger emission area is observed in both devices compared to the pumping spot (230 μm in diameter) (Figure 5g).

3. Conclusion

We have studied the exotic chiral characteristics of a lasing system constituted by a thin layer of dye-doped-resist embedded within two CNC layers. The scattering strength of the second CNC film has been enhanced by mixing in different fractions of SiO_2 spheres (600 nm). The properties of the CNC and SiO_2-CNC layers were investigated in terms of their transmittance, g-factor, and polarimetric analysis. Even after the introduction of SiO_2 NPs, the cholesteric structure of the CNC assembly was maintained, with the g-factor reaching its maximum at 1.33 for 4 wt.% thanks to a conversion of linear diattenuation to circular diattenuation response caused by the silica-CNC composites. In this sense D_L decreased 7 times from 0.42 to 0.06 for the highest concentration of silica considered (4 wt.%), indicating the lowest linear diattenuation property. We then used these bare and silica-doped CNC films to build a chiral lasing system by placing a thin layer of active material between two CNC film layers, the second of which contained different fractions of silica. This lasing configuration exhibited the highest g_{lum} up of 0.6 above its threshold by benefitting from the light amplification provided by the SiO_2/CNC layer. The chiral lasing devices showed multidirectional emission originated by the diffusive medium and maintained their g_{lum} until 30°. This chiral laser system exploits biopolymeric materials provided in nature, enabling it to be applied in various fields from optical communications to therapeutic techniques. Moreover, these CNC-silica layers can be easily implemented in commercial optoelectronic devices such as LEDs to seamlessly produce chiral lasing without the need for bulky optics.[43]

4. Experimental Section

Reagents: Rhodamine B (M_W 479.01 g mol^{-1}) and Polyether-sulfone (PES) membranes (220 nm pore size, Millipore Express PULS) were purchased from Sigma–Aldrich. Nanocrystalline Cellulose (CNC) powder (Diameter: 10–20 nm, Length: 300–900 nm) was purchased from Nanografi. Deionized (DI) water (resistivity, 18.2 MΩ) was obtained from a reverse osmosis system. The negative photoresist SU8-2000.5 (14% solid) and the SU8-2000 thinner were purchased from MicroCHEM resists. The glass substrates were purchased from TED Pella (Microscope slides 3" × 2").

Fabrication and Transfer of CNC Films: Four wt.% of a CNC stock solution was prepared by putting 25 g of CNC powder into 100 mL of DI water. To disperse it uniformly, the dispersion was stirred overnight after an hour of sonication in a sonic bath (2800-CPXH, Branson). The stock solution was diluted to 1 wt.% by adding DI water. Tip sonication (VCX-500, Sonics & Materials Inc.) was conducted with 2.5 Kj /g_{CNC} to obtain uniform dispersions by breaking residual agglomerated particles and then left for 24 h to stabilize. The 600 nm diameter SiO_2 spheres were synthesized by the Stöber method, washed in water and ethanol, and dried. The silica powder was added into the 1 wt.%. CNC solution targeting SiO_2 concentration from 1.25. to 4 wt.%.

The CNC films were prepared by placing 15 mL of CNC solution on a PES membrane and using a vacuum filtration system for several hours. The membrane was transferred onto a glass substrate previously cleaned with oxygen plasma for 10 min. After the drying process, the membrane was carefully peeled off from the system.

Device Fabrication: The first film of CNC, the bare CNC film on glass, was used as a substrate onto which the subsequent layers were deposited. To make the active layer, 5.25 mg of Rhodamine B was dissolved into 1 mL of SU8-thinner, and mixed with SU8 2000.5 photoresist (14% in thinner) in a 1:1 ratio. After sonication in a sonic bath for 15 min, it was kept under stirring for several hours. The RhB-SU8 mixture was spin-coated (10s at 500 rpm and 30s at 2000 rpm) onto a bare CNC film. The composite film was heated on a hotplate at 60 °C for 2 min to remove residual solvents. Next, the sample was cured under UV exposure for 25 min. The cured CNC-RhB-SU8 composite was cut into 5 × 20 mm pieces and detached

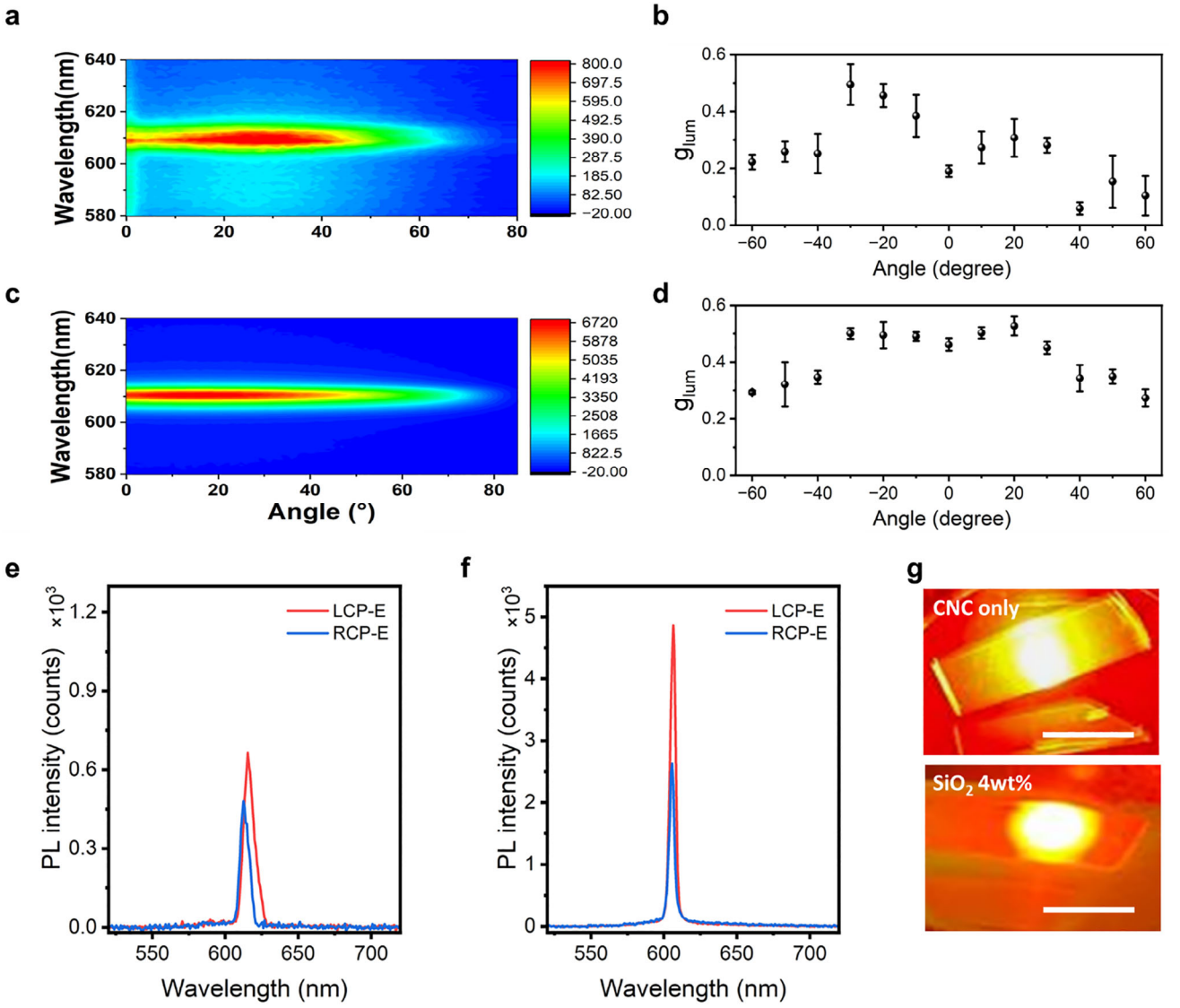

Figure 5. Angular distribution for LCP emission and its corresponding g_{lum} values for the a,b) CNC/RhB/CNC and c,d) CNC/RhB/CNC/SiO_2 (4 wt.%) films. Photoluminescence Intensity for left and right-handed circular polarizations collected at 20° for the e) CNC/RhB/CNC and f) CNC/RhB/CNC/SiO_2 (4 wt.%) films. g) Optical images from both bare CNC and silica-doped CNC systems under optical excitation (scale bars:1 cm) All PL measurements were collected under 110.67 μJ mm^{-2}.

from the glass substrate. The completed CNC films with the active layer were put on pre-wetted bare CNC or CNC-SiO_2 composite films and left to dry under ambient conditions overnight. The schematic description can be found in Figure S1 (Supporting Information).

SEM Measurement: The cross-sectional images of the bare CNC and its composite films were obtained with a field emission scanning electron microscope (FE-SEM, Magellan 400L, FEI Co.), with an acceleration voltage of 2 kV.

CD Measurement: All optical measurements were taken in a custom-built experimental setup. The sample was illuminated with white light from a Tungsten Halogen lamp (Ocean Optics, HL-2000-HP, Florida, USA) at normal incidence. The white light passed through a Glen–Thompson linear polarizer (GTH10, Thorlabs) and a super achromatic quarter wave-plate (SAQWP05M-700, Thorlabs) at ± 45° to generate CPL. The transmitted light was collected by a fiber-connected spectrophotometer (Ocean Optics, QEPro-FL) with a range of detection 380–1200 nm. The CD measurements were fully automated with a Labview program. The schematic for this measurement setup available in Figure S7 (Supporting Information).

Mueller Matrix Analysis: The Mueller matrix images were collected with a custom-built experimental setup (complete Mueller matrix image polarimeter). The red LED source (633 nm) followed by a 5 nm band-pass filter illuminates the sample after passing through a polarization state generator (PSG) able to generate any fully polarized state of polarization. After light-matter interaction, exiting light was analyzed by a polarization state analyzer (PSA). The PSG includes a linear polarizer (CASIX, Glan–Thompson polarizer) and two parallel-aligned liquid crystal retarders (Meadowlark Optics, LVR-200-400-700-1LTSC). For the PSA, all components were identical to the PSG but arranged in reverse order. After PSA, a CCD camera (G-504B CCD camera, Vision manta) was placed to measure MM data. More details of the setup and background theory can be found in Section S2 (Supporting Information).

Lasing Characterization: The samples were optically pumped by a nanosecond-pulsed green laser with one pulse (CryLaS Gmb, FDSS 532-

150), peaked at 532 nm with a repetition rate of 100 Hz, and linearly polarized. To assess their lasing threshold and slope efficiency, the laser power was increased from 200 to 500 μW, which was measured by an optical power meter console (Thorlabs PM100D) with a photodiode power sensor (Thorlabs S121C). The optical excitation beam diameter (230 μm) was measured by a beam profiler (BP209-VIS/M, Thorlabs) to calculate the pumping energy density. For CPL measurements, the optical pumping was focused on the sample and collected using a pair of achromat 4x objective lenses (NA = 0.10, WD = 18.5 mm). The light passed through a Glen–Thompson linear polarizer and a super achromatic quarter-wave plate mounted on a rotation mount (ELL14, Thorlabs) to measure the CPL signal. The CPL measurements were fully automated with a Labview program.

Polarization and Angular Characterization: For the polarization study, the PL emission excited by the green laser passed through an achromatic quarter wave plate (AHWP10M-600, Thorlabs) at −45° from the fast axis and a wire-grid linear polarizer. (WP25M-VIS, Thorlabs). The emission passed through a rotating linear polarizer from 0° to 180°, referred to as the same rotation direction of the quarter-wave plate. (Figure S7, Supporting Information). For the angular characterization, Arduino controlled rotational stage was applied on the same optical setup for the polarization study (Figure S8, Supporting Information). The rotational stage was controlled by a customized Labview program. All PL measurements for the polarization and the angular studies were carried out at the pumping energy density of 110.67 μJ mm^{-2}.

Supporting Information

Supporting Information is available from the Wiley Online Library or from the author.

Acknowledgements

This work had received funding from the Spanish Agencia Estatal de Investigación/ Spanish Ministry of Science and Innovation (AEI/MCIN) through grants PID2022-141956NB-I00 MCIN/AEI/10.13039/501100011033(OUTLIGHT), and CEX2019-000917-S (FUNFUTURE, Spanish Severo Ochoa Centre of Excellence program) and from the Generalitat de Catalunya (2021-SGR-00444). This research was also kindly supported by the European Union through the ERC Proof of Concept 101069234 (CELLO) and the EIC PATHFINDER OPEN project 101046489 (DYNAMO). J.C., I.E., and A.L. acknowledge funding by the Ministerio de Ciencia de Innovación and Fondos FEDER (PID2021-126509OB-C21).

Conflict of Interest

The authors declare no conflict of interest.

Data Availability Statement

The data that support the findings of this study are available from the corresponding author upon reasonable request.

Keywords

chiral nematic structure, circularly polarized light, crystalline nanocelluloses, mueller matrix

Received: January 20, 2025
Revised: April 1, 2025
Published online: April 21, 2025

[1] Y. Zhao, Y. Yao, K. Xu, Y. Yang, J. Tian, *Opt. Commun.* **2020**, *475*, 126165.
[2] Y. Chen, X. Yang, J. Gao, *Light Sci. Appl.* **2019**, *8*, 45.
[3] X. Zhan, F. F. Xu, Z. Zhou, Y. Yan, J. Yao, Y. S. Zhao, *Adv. Mater.* **2021**, *33*, 2104418.
[4] A. Qu, L. Xu, C. Xu, H. Kuang, *Chem. Commun.* **2022**, *58*, 12782.
[5] J. Mendoza-Carreño, P. Molet, C. Otero-Martínez, M. I. Alonso, L. Polavarapu, A. Mihi, *Adv. Mater.* **2023**, *35*, 2210477.
[6] N. Fiuza-Maneiro, J. Mendoza-Carreño, S. Gómez-Graña, M. I. Alonso, L. Polavarapu, A. Mihi, *Adv. Mater. 36*, 2413967.
[7] I. C. Seo, Y. Lim, S.-C. An, B. H. Woo, S. Kim, J. G. Son, S. Yoo, Q.-H. Park, J. Y. Kim, Y. C. Jun, *ACS Nano* **2021**, *15*, 13781.
[8] K. Konishi, M. Nomura, N. Kumagai, S. Iwamoto, Y. Arakawa, M. Kuwata-Gonokami, *Phys. Rev. Lett.* **2011**, *106*, 057402.
[9] W. Dai, Y. Wang, R. Li, Y. Fan, G. Qu, Y. Wu, Q. Song, J. Han, S. Xiao, *ACS Nano* **2020**, *14*, 17063.
[10] Y. Yang, R. C. da Costa, M. J. Fuchter, A. J. Campbell, *Nat. Photonics* **2013**, *7*, 634.
[11] E. M. Sánchez-Carnerero, A. R. Agarrabeitia, F. Moreno, B. L. Maroto, G. Muller, M. J. Ortiz, S. de la Moya, *Chem. – Eur. J.* **2015**, *21*, 13488.
[12] B. Tang, S. Wang, H. Liu, N. Mou, A. S. Portniagin, P. Chen, Y. Wu, X. Gao, D. Lei, A. L. Rogach, *Adv. Opt. Mater.* **2024**, *12*, 2301524.
[13] S. Lee, Y.-C. Lim, H. Kim, D. Hye Seo, J. Na, H. Kim, K. Tae Nam, Y. Jeong, *ACS Photonics* **2022**, *9*, 613.
[14] B. Frka-Petesic, S. Vignolini, *Nat. Photonics* **2019**, *13*, 365.
[15] Y. Dong, C. Rossner, A. Fery, *ACS Appl. Opt. Mater.* **2023**, *1*, 1862.
[16] S. Farooq Adil, V. S. Bhat, K. M. Batoo, A. Imran, M. E. Assal, B. Madhusudhan, M. Khan, A. Al-Warthan, *J. Saudi Chem. Soc.* **2020**, *24*, 374.
[17] C. M. Walters, C. E. Boott, T. D. Nguyen, W. Y. Hamad, M. J. Maclachlan, *Biomacromolecules* **2020**, *21*, 1295.
[18] G. Guidetti, S. Atifi, S. Vignolini, W. Y. Hamad, *Adv. Mater.* **2016**, *28*, 10042.
[19] S. Beck, J. Bouchard, R. Berry, *Biomacromolecules* **2010**, *12*, 167.
[20] Q. Chen, P. Liu, F. Nan, L. Zhou, J. Zhang, *Biomacromolecules* **2014**, *15*, 4343.
[21] R. M. Parker, G. Guidetti, C. A. Williams, T. Zhao, A. Narkevicius, S. Vignolini, B. Frka-Petesic, *Adv. Mater.* **2018**, *30*, 1704477.
[22] R. Prathapan, R. F. Tabor, G. Garnier, J. Hu, *ACS Appl. Bio Mater.* **2020**, *3*, 1828.
[23] C. Li, J. Evans, N. Wang, T. Guo, S. He, *Sci. Rep.* **2019**, *9*, 11290.
[24] R. M. Parker, T. H. Zhao, B. Frka-Petesic, S. Vignolini, *Nat. Commun.* **2022**, *13*, 3378.
[25] T. H. Zhao, R. M. Parker, C. A. Williams, K. T. P. Lim, B. Frka-Petesic, S. Vignolini, *Adv. Funct. Mater.* **2019**, *29*, 1804531.
[26] G. Antonopoulos, G. Kakarantzas, *Mater. Res. Express* **2019**, *6*, 1150d9.
[27] A. Querejeta-Fernández, B. Kopera, K. S. Prado, A. Klinkova, M. Methot, G. Chauve, J. Bouchard, A. S. Helmy, E. Kumacheva, *ACS Nano* **2015**, *9*, 10377.
[28] E. Lizundia, T. D. Nguyen, J. L. Vilas, W. Y. Hamad, M. J. Maclachlan, *Mater. Chem. Front.* **2017**, *1*, 979.
[29] R. Xiong, S. Yu, M. J. Smith, J. Zhou, M. Krecker, L. Zhang, D. Nepal, T. J. Bunning, V. V. Tsukruk, *ACS Nano* **2019**, *13*, 9074.
[30] D. Qu, M. Archimi, A. Camposeo, D. Pisignano, E. Zussman, *ACS Nano* **2021**, *15*, 8753.
[31] F. Zhang, Q. Li, C. Wang, D. Wang, M. Song, Z. Li, X. Xue, G. Zhang, G. Qing, *Adv. Funct. Mater.* **2022**, *32*, 2204487.
[32] M. Kim, H. Lee, R. T. Snipes, M. J. Han, V. V. Tsukruk, *Small* **2022**, *18*, 2104340.
[33] A. Mendoza-Galván, E. Muñoz-Pineda, S. J. L. Ribeiro, M. V. Santos, K. Järrendahl, H. Arwin, *J. Opt.* **2018**, *20*, 2.

[34] H. Arwin, S. Schoeche, J. Hilfiker, M. Hartveit, K. Järrendahl, O. R. Juárez-Rivera, A. Mendoza-Galván, R. Magnusson, *Appl. Sci.* **2021**, *11*, 6742.
[35] W. Stöber, A. Fink, E. Bohn, *J. Colloid Interface Sci.* **1968**, *26*, 62.
[36] F. C. MacKintosh, J. X. Zhu, D. J. Pine, D. A. Weitz, *Phys. Rev. B* **1989**, *40*, 9342.
[37] M. Xu, R. R. Alfano, *Phys. Rev. E* **2005**, *72*, 065601.
[38] J. J. Gil, E. Bernabeu, *Opt. Acta Int. J. Opt.* **1986**, *33*, 185.
[39] G. Chu, X. Wang, T. Chen, W. Xu, Y. Wang, H. Song, Y. Xu, *J. Mater. Chem. C* **2015**, *3*, 3384.
[40] H. Zheng, B. Ju, X. Wang, W. Wang, M. Li, Z. Tang, S. X. A. Zhang, Y. Xu, *Adv. Opt. Mater.* **2018**, *6*, 1801246.
[41] S. Zhao, Y. Yu, B. Zhang, P. Feng, C. Dang, M. Li, L. Zhao, L. Gao, *Colloids Surf. Physicochem. Eng. Asp.* **2022**, *645*, 128921.
[42] H. Agha, Y. Geng, X. Ma, D. I. Avşar, R. Kizhakidathazhath, Y.-S. Zhang, A. Tourani, H. Bavle, J.-L. Sanchez-Lopez, H. Voos, M. Schwartz, J. P. F. Lagerwall, *Light Sci. Appl.* **2022**, *11*, 309.
[43] A. Consoli, N. Caselli, C. López, *Nat. Photonics* **2022**, *16*, 219.